ACS OMEGA

http://pubs.acs.org/journal/acsodf

Article

Stretchable Conductive Tubular Composites Based on Braided Carbon Nanotube Yarns with an Elastomer Matrix

Avia J. Bar,* Joey Mead, Hanna Dodiuk, and Samuel Kenig

Cite This: *ACS Omega* 2022, 7, 40766−40774

Read Online

ACCESS | Metrics & More | Article Recommendations | Supporting Information

ABSTRACT: We report an innovative approach to creating stretchable conductive materials composed of a tubular shell made from braided carbon nanotube yarns (CNTYs) embedded in an elastomeric matrix. For stretchable electronics, both mechanical properties and electrical conductivities are of interest. Consequently, both the mechanical behavior and electrical conductivities under large deformations were investigated. A new hyperelastic composite model was developed to predict the large deformation response to applied stress for a braid in a tubular elastomer composite. The composite demonstrated a hyperelastic response due to the architecture of the braid, and the behavior was affected by the braiding angle, braid modulus, and volume fraction of fibers. The elastomer matrix was considered a neo-Hookean material and represented by the Yeoh model. An interaction parameter was proposed to account for the effect of the elastomer/braid cooperative restriction as observed in experimental and calculated results. This novel approach enabled the determination of the constitutive behavior of the composite in large deformations (>150%), taking into account the elastomer and yarn properties and braid configurations. The model exhibited good agreement with the experimental results. As the CNTYs are conductive, a stretchable conductive composite was obtained having a resistivity of 5.01×10^{-4} and 5.67×10^{-5} Ω·cm for the 1-ply and 4-ply composites, respectively. The resistivity remained constant through cyclic loading under large deformations in tension until mechanical failure. The material has potential for use in stretchable electronics applications.

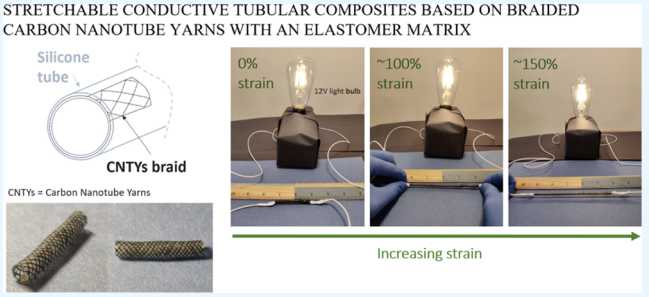

INTRODUCTION

Stretchable electronics should comprise simultaneously of highly deformable and conductive elements with low permanent set and constant electrical conductivity. Basic studies related to stretchable electronics started two decades ago[1] and have continued to expand.[2−6] There are numerous applications for stretchable electronics, such as healthcare monitors,[7−10] artificial skins,[11−13] human−machine interfaces,[14] wearable electronics,[15] and others.[16,17] Preferably, the stretchable conductive material should be lightweight, especially for wearable devices, to achieve maximum comfort for weight-sensitive applications. The basic requirements for stretchable conductive materials are to maintain high constant conductivity under large deformations while returning to the original size without permanent set[18] with the potential for scaling up to large area parts.[18] These requirements can be met using conductive particles/short fibers or using conductive reinforcements in woven, knitted, braided, or other forms. Short fibers and particulate systems have been used for stretchable conductive materials; however, the distance between the conductive moieties increases at large strains, leading to decreased conductivities.[19] Hence, to accomplish large deformations of the elastomeric composite, while maintaining high conductivity, the conductive fibers must be able to deform with the matrix and remain continuous.

Consequently, an innovative approach is proposed that consists of a tubular shell made of braided carbon nanotube yarns (CNTYs) embedded in an elastomeric matrix. Embedded braids are commonly used for reinforced hoses, catheters, etc.[20−23] In these applications, the braid's primary purpose is to reinforce the shell structures. However, the stretchability is limited in these applications. For stretchable electronics, both electrical conductivities and mechanical properties are of interest. In this work, poly(dimethylsiloxane) (PDMS) was selected due to its high stretchability, a large working temperature range, good dielectric properties, electrical insulation, hydrophobicity, and the ability to form good bonding[24] with carbon-based materials.[25] For the conductive element, many options can be considered, including metals like copper, gold, silver, and iron and carbon nanotube yarns.[26] The advantages of CNTYs are attributed to their low specific weight combined with high flexibility and electrical and thermal

Received: March 31, 2022
Accepted: September 14, 2022
Published: November 7, 2022

https://doi.org/10.1021/acsomega.2c01991
ACS Omega 2022, 7, 40766−40774

conductivities. The present study was based on PDMS and CNTYs for stretchable conductive applications. For fiber placement configurations, braiding was chosen due to its ability to combine highly stretchable yarn by changing the interyarn angle and the ability to adjust the content levels of the braided material in a continuous scalable production method.

The mechanical behavior of the CNTYs/elastomer composites under varying and repeatable stresses under large deformation is of utmost importance. The existing mechanical modeling for polymer/fiber composites is based on classical laminate plate theory, fabric geometry models (FGMs), finite-element analysis, and volume averaging methods, which are reviewed in detail by Carey.[27] Commonly, these models predict the final properties of the composite braid. Other models[28−31] describing rubber-reinforced fabric composites are founded on energy considerations and use experimental data in different directions to determine the number of constants needed to define the constants of the composite using approaches similar to rubber modeling. Energy-based models require significant experimental testing and data to provide the appropriate constants for the model.

The existing models for elastomer fiber composites are not applicable at high deformations; hence, for stretchable conductive materials, advanced models are required. Consequently, a novel model was developed to predict the mechanical behavior in the uniaxial direction for braided CNTYs and elastomer composites at high deformations. Concurrently, with the high level of mechanical stretching, the electrical conductivity has to be maintained. As a result, the conducting component of the composite element has to sustain its continuity and thus has to change its configuration with stretching. Therefore, a braided structure is investigated as a means to meet these requirements.

Mechanical Modeling. The investigation starts with mechanical characterization and modeling of the tubular elastomeric composite. The model is based on the rule of mixtures and considers the contributions of the braided CNTYs and the elastomer matrix to the stresses under large deformations.

The approach in the present investigation for predicting the axial stress development during large elongations in the axial direction is based on FGMs combined with hyperelastic material theory proposed by Yeoh.[32] The model defines a critical strain, $\varepsilon_{z,c}$, below which the composite behaves similarly to the neat elastomer and above which the stretched yarns make a significant contribution to stress-bearing in the composite. An interaction parameter was specified to account for the interactive restriction between the elastomer and the braid.

The modeling of the tubular braid composite is based on the assumption that the braiding has an open mesh structure and is located in the middle of the tube wall with no twist occurring during the stretch. Each yarn is assumed to follow a helical path and is linearly elastic with a modulus of E_0, having small displacements compared to the elastomer strains. Furthermore, it was assumed that the volume of the braided structure is conserved under tension; concerning the elastomer, it has been assumed that it is incompressible and follows the 'Yeoh model' (for an incompressible material and uniaxial strain) with a Poisson's ratio close to 0.5.

The overall schematics of the model and the actual tubular composite are described in Figure 1.

The model proposes that the entire stretching span can be divided into two ranges. In "range I", for relatively low deformations and below a critical strain $\varepsilon_{z,c}$, the elastomer dominates the stress/strain behavior, and in "range II", which is above the critical strain, the yarns dominate the stress−strain behavior of the elastomeric composite.

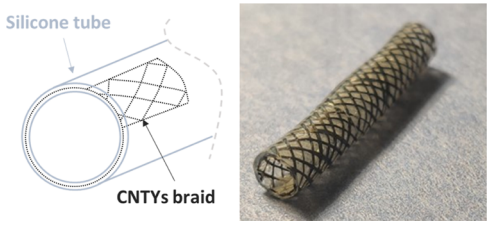

Figure 1. Schematic image of stretchable tubular CNTYs embedded in silicone rubber.

In range I, the effective axial stress is determined predominantly by the contribution of the elastomer matrix. The tensile stress on the coreless tubular structure is given by

$$\sigma_{\text{composite}} = \sigma_{\text{r}} \tag{1}$$

where σ_{r} is the engineering stress of the rubber (elastomer).

In range II, the effective axial stress is determined by the contribution of the matrix and CNTYs. The tensile stress on the coreless tubular structure is given by

$$\sigma_{\text{composite}} = (1 - \phi)\sigma_{\text{r}} + \phi\frac{F_{\text{b}}}{A_{\text{b}}} \tag{2}$$

where F_{b} is the axial force extending the braid, A_{b} is the initial cross section of the braid, and ϕ is the volume fraction of the braid. The volume fraction of the braided CNTYs is ϕ and shown in eq 3 (see Supporting Information 1)

$$\phi = \frac{v_{\text{f}}}{v_{\text{c}}} = \frac{N}{\cos(\alpha_{\text{i}})}\frac{d_{\text{y}}^2}{(d_{\text{o}}^2 - d_{\text{i}}^2)} \tag{3}$$

where v_{f} is the volume of fibers (yarns), v_{c} is the volume of the composite, α_{i} is the initial braiding angle, N is the number of yarns, d_{y} is the diameter of the yarn, and d_{o}, d_{i} are the outside and inside diameter of the tube, respectively.

The Yeoh model is based on a phenomenological description of the observed behavior for the deformation of nearly incompressible, elastic, and uniaxial strain as follows[32]

$$\sigma_{\text{r}} = 2\left(\lambda - \frac{1}{\lambda^2}\right)\frac{\partial w}{\partial I_1} \tag{4}$$

where λ is the axial extension and $\frac{\partial w}{\partial I_1}$ includes a summation of n terms and is written as

$$\frac{\partial w}{\partial I_1} = \sum_{i=1}^{n} iC_i(I_1 - 3)^{i-1} \tag{5}$$

where C_i are material constants. The constants can be determined by fitting a uniaxial tensile stress−strain curve of neat rubber. The strain invariant, I_1, is defined based on assuming incompressibility and for uniaxial tension, $\lambda_1 = \lambda$ and $\lambda_2 = \lambda_3$, as

$$I_1 = \lambda^2 + \frac{2}{\lambda} \tag{6}$$

The axial force component of the braid is the total axial force acting on the yarns and is given by

https://doi.org/10.1021/acsomega.2c01991
ACS Omega 2022, 7, 40766−40774

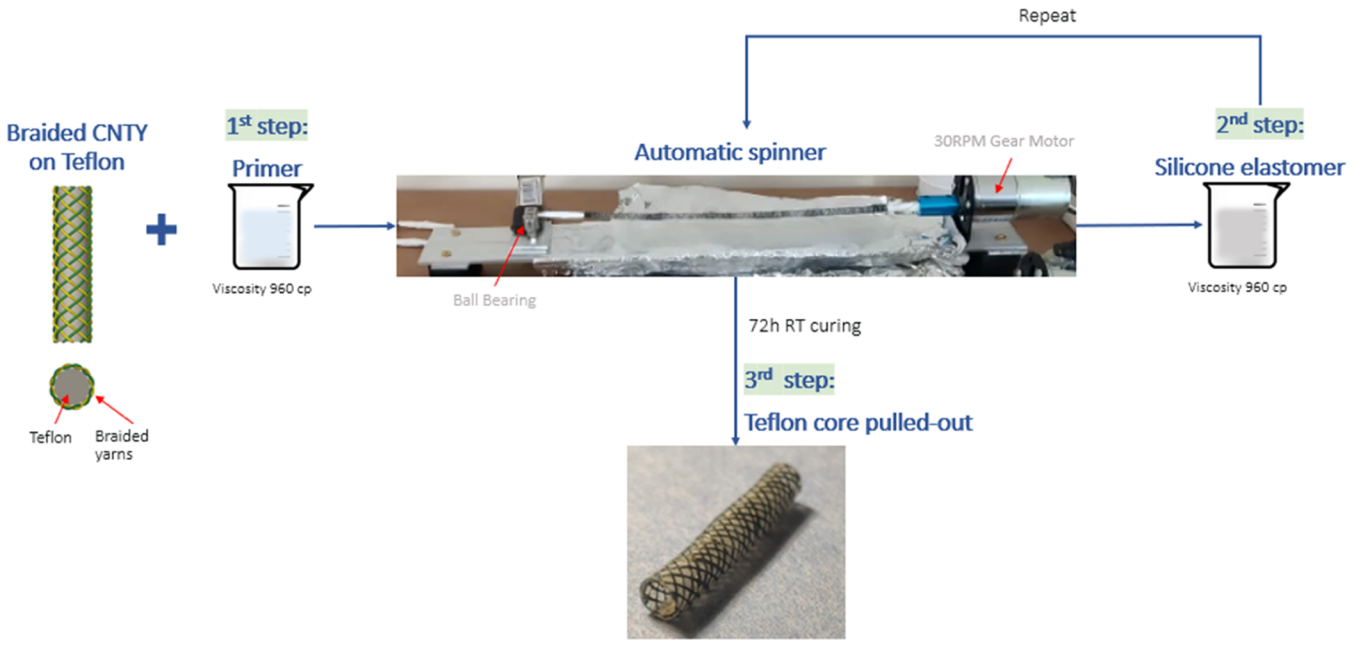

Figure 2. Process schematics for the stretchable tubular composite by rotating the braided yarns around a Teflon core.

$$F_b = N\varphi_y F_f \cos(\alpha) \tag{7}$$

where F_f is the filament tension, α is the braiding angle, and φ_y is the yarn packing factor defined as the ratio of the volume of constituent filaments to the yarn volume. For the yarn in tension, the axial force is[33]

$$F_f = f(\varepsilon_f) \tag{8}$$

where ε_f is the yarn strain. The yarn strain was assumed to follow Hookean elastic behavior. The axial strain and the yarn strain can be related using the geometry of a helical wrapping. Thus, according to Rawal et al.[34,35] and including an interactive-restraining parameter ζ, the strain in the fiber, ε_f, is

$$\varepsilon_f = \left[(1 + \zeta\varepsilon_z)^2\cos^2(\alpha_i) + \frac{\sin^2(\alpha_i)}{(1 + \zeta\varepsilon_z)}\right]^{0.5} - 1 \tag{9}$$

The effective cross-sectional area of the braid (A_b) is (see Supporting Information 2)

$$A_b = \frac{N\pi d_f^2(C + 1)}{4\cos(\alpha_i)} \tag{10}$$

where C is the fiber crimp and d_f is the fiber diameter.

Combining eqs 2−10, the following relationship is obtained for the effective tensile stress

$$\sigma_{composite} = \left(1 - \frac{N}{\cos(\alpha_i)}\frac{d_y^2}{(d_o^2 - d_i^2)}\right)2\left(\lambda - \frac{1}{\lambda^2}\right)\sum_{i=1}^{n} iC_i\left(\lambda^2 + \frac{2}{\lambda} - 3\right)^{i-1} + \left(\frac{N}{\cos(\alpha_i)}\frac{d_y^2}{(d_o^2 - d_i^2)}\right)\frac{4N\varphi_y F_f \cos(\alpha)\cos(\alpha_i)}{(d_o^2 - d_i^2)(C + 1)\pi} \tag{11}$$

The braiding angle (α) changes during stretching and was calculated using the following equation

$$\cos(\alpha) = \frac{1 + \zeta\varepsilon_z}{1 + \varepsilon_f}\cos(\alpha_i) \tag{12}$$

In a composite, the strain of one component may be limited by the strain of the second component, assuming a certain degree of interaction between the two components. In the elastomer composite braid, the braid is restrained by the elastomer matrix, and the elastomer is restrained by the braid. Considering only two configurations for the elastomer, a rod and a tube, the change in the diameters will be different. For a tube geometry, the ratio of the instantaneous diameter, D, to the initial diameter, D_0, where D and D_0 are the normalized diameters (which can be taken as the average of the inner and outer diameters) vs the axial strain is expressed in eq 13. For a rod geometry or an elastomer strand, the ratio vs axial strain is given by eq 14

$$\frac{D}{D_0} = (1 - \nu\varepsilon_z) \tag{13}$$

$$\left(\frac{D}{D_0}\right)^2 = \frac{1}{(1 + \varepsilon_z)} \tag{14}$$

where ν is the Poisson's ratio assumed to be 0.5. The ratio of the instantaneous diameter to the initial diameter of the braid, d/d_0, is related to the initial braid angle and the extension as expressed in eq 15

$$\frac{d}{d_0} = \frac{1}{\tan(\alpha_i)}\left(\frac{1}{\cos^2(\alpha_i)} - (1 + \varepsilon_z)^2\right)^{0.5} \tag{15}$$

EXPERIMENTAL SECTION

Materials. For the fibers, CNTYs (Miralon yarn, Nanocomp Technologies, Inc. Merrimack, New Hampshire) were used.[26] The materials were a direct-spun untreated single-ply CNTY with a linear density of 10 tex (10 g/km) and a diameter of ∼150 μm (Nanocomp A-series) and post-treated four-ply CNTYs that were stretched in the presence of acids by the manufacturer with

https://doi.org/10.1021/acsomega.2c01991
ACS Omega 2022, 7, 40766−40774

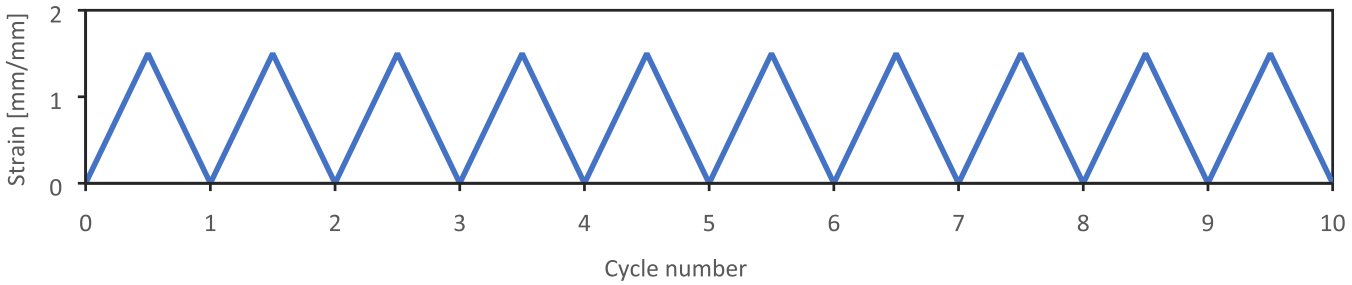

Figure 3. Extension profile for the electrical measurement.

a linear density of 29 tex and a diameter of ~240 μm (Nanocomp C-series).

A silicone elastomer (DOW DOWSIL 92-009 Dispersion Coating Clear manufactured by Dow Inc.) was used as the elastomer matrix material. The silicone elastomer was diluted 1 part in a 4:3 (v/v) ratio with a naphtha thinner (Varnish Maker and Painter's Naphtha manufactured by Klean-strip). A primer (DOW DOWSIL 1200 OS PRIMER CLEAR 309 G BOTTLE manufactured by Dow Inc) was used to treat the CNTYs prior to coating with the silicone matrix to improve silicone bonding to the yarns.

Composite Preparation Method. The braiding of the CNTYs was carried out using a braiding machine (Wardwell Braiding Co. Central Falls, Rhode Island) with 16 rotating CNTYs (130 and 240 μm). A range of tubular shell braids was fabricated using rigid Teflon rods to define the inside diameter of the tubular braid. As shown in Figure 2, the braided CNTYs were coated with the silicone elastomer. The impregnation of the braided CNTYs was carried out by dipping the braid on the Teflon core in the silicone elastomer solution and then applying a 30 rpm rolling motion, creating a composite with an elastomer matrix. The matrix coating was carried out in stages, layer by layer (9 layers), and with each layer allowed to dry in ambient air for up to 2 h prior to application of the next layer. Final curing was at RT for 72 h. The edges of the samples were covered to avoid impregnation of the matrix for measurement of electrical properties.

The composite tensile load−deformation relationship was studied using a mechanical tester (Instron4466, Instron, Norwood, Massachusetts), with a 2 kN load capacity. The displacement of the grips was used to calculate the strain, assuming a gauge length of 40 mm. The samples were subjected to 10 cycles of stretching/relaxation to predetermined strain values at a rate of 100 mm/min while simultaneously measuring the electrical resistance. At least three samples were tested under the same conditions for each loading procedure. After 2 weeks of recovery, some tests were also done to study the stress−strain and electrical relationship after long-term relaxation.

The electrical resistance was measured simultaneously with stress−strain measurements during the extension and relaxation cycles. The composite samples were subjected to 10 cycles (Figure 3) of stretching/relaxation using strain rates of 100 cm/min. At least three specimens were characterized under the same conditions for each result. The electrical properties of the CNTYs were measured using a two-probe electrical resistance device (FLUKE 179 multimeter). The applied voltage was 5 kV. The measuring probes were connected by conductive tapes (copper foil) applied to the yarn to achieve good contact between the CNTYs and the probes. An insulating layer between the CNTYs/conductive tape and the clamps was included for insulation. The properties (electrical and mechanical) for the CNTYs were calculated using the measured cross-sectional area (datasheets from Nanocomp) and referred to as "apparent" properties.

RESULTS AND DISCUSSION

According to eqs 13−15, the change in diameters with strain for both the tube and rod geometries and the ratio of the instantaneous diameter to the initial diameter of the braid, d/d_0, was calculated with an initial braiding angle of 55° and compared to the experimental results. As shown in Figure 4, the experimental results are close to the stretching behavior of the neat tube rubber rather than the change in diameter of the braid.

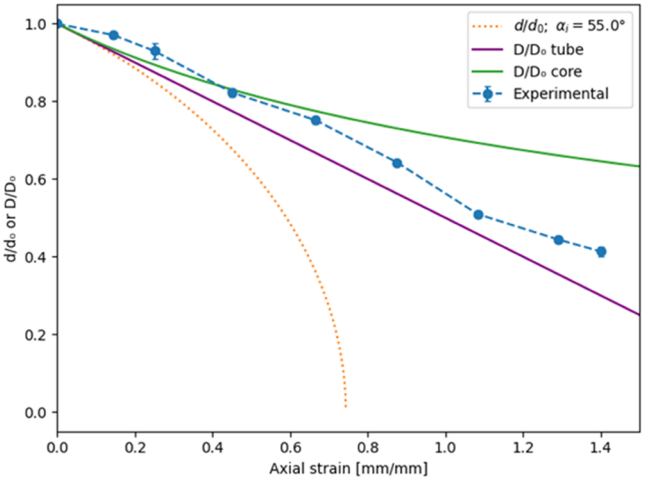

Figure 4. Variation of elastomer diameter, braid diameter, and experimental results with axial strain.

As can be deduced from Figure 4, the diameter differences between the neat elastomer and the neat braid increase with stretching, indicating that the interaction between these two opposing components increases with the level of strain. Hence, to describe the actual diameter decrease of the composite diameter and stress−strain relationship, an interaction parameter should be introduced to describe the behavior at high strains.

The interaction parameter was considered to be an interaction-restraining function, $\zeta(\varepsilon_z)$, which was defined as a function of strain. An iterative procedure was used to obtain the $\zeta(\varepsilon_z)$ function by minimizing the difference between the experimental and the computational stresses. The $\zeta(\varepsilon_z)$ function was determined only for the second range, where the strain was greater than the critical strain.

The potential failure modes (or limiting conditions) of braided composites are depicted in Figure 5 and can be used to

https://doi.org/10.1021/acsomega.2c01991
ACS Omega 2022, 7, 40766−40774

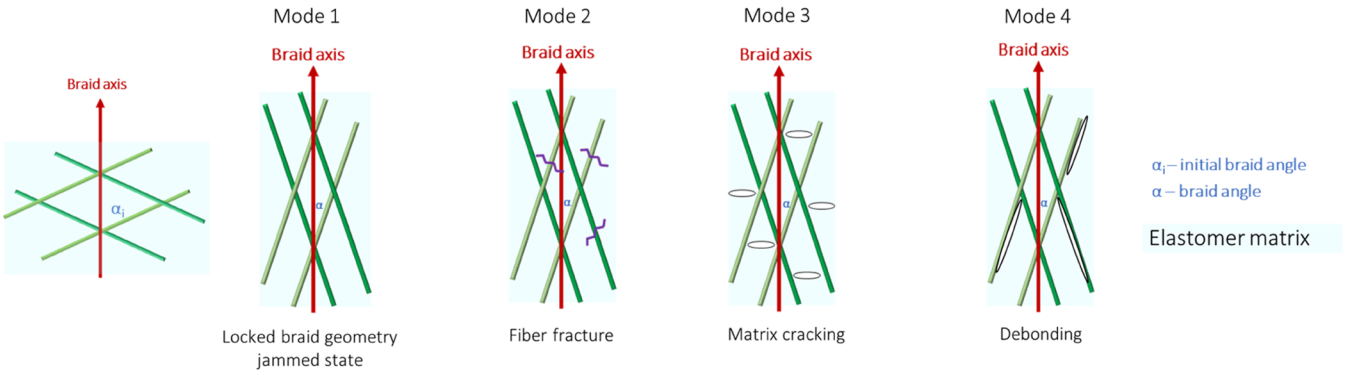

Figure 5. Four failure modes.

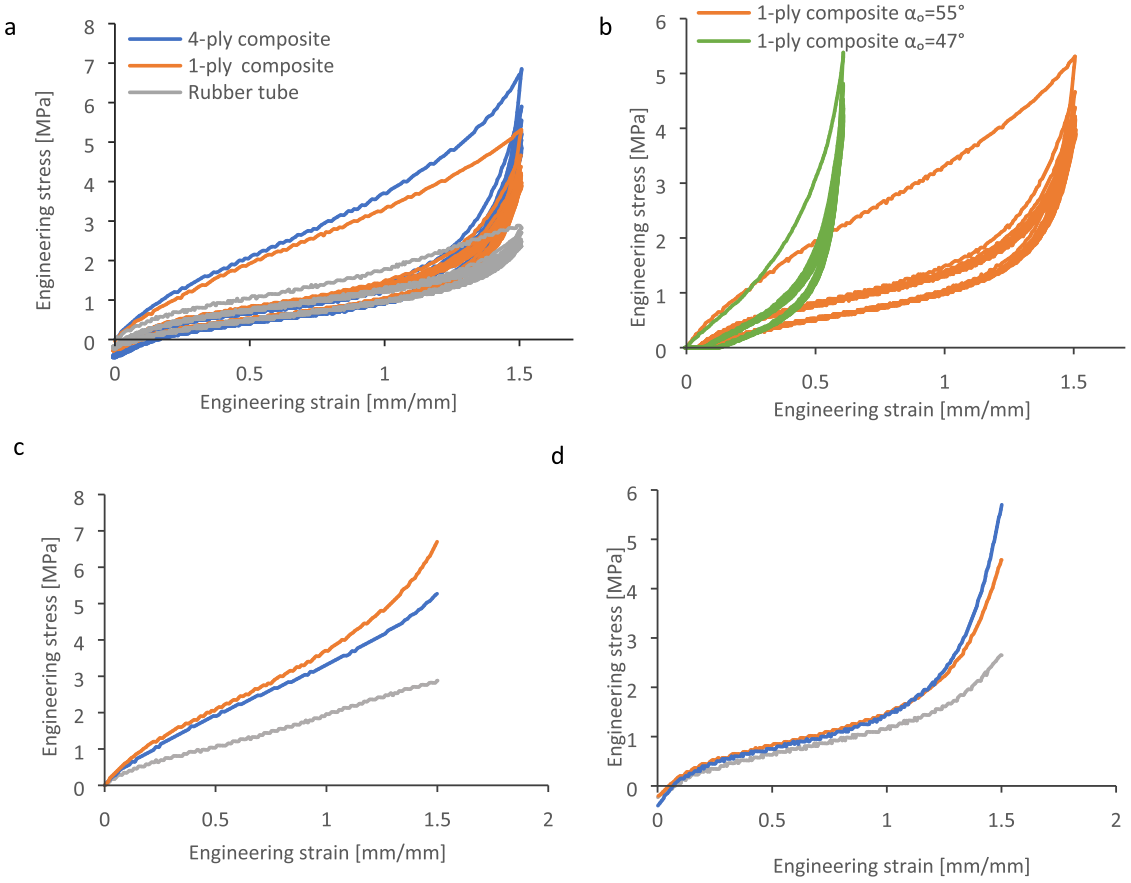

Figure 6. Relationship between strain and stress: (a) 10 cycles for neat rubber and the stretchable 1-ply and 4-ply CNTY composites with a braiding angle of 55°; (b) 10 cycles for the stretchable 1-ply CNTY composites with braiding angles of 55 and 47°; for neat rubber and the stretchable 1-ply and 4-ply CNTY composites with a braiding angle of 55° (c) loading of the first cycle; and (d) loading of the second cycle.

Table 1. Hysteresis of Neat Elastomer and Elastomer CNTYs Braided with 1-ply and 4-ply for Different Loading Cycles

	1st cycle (%)	2nd cycle (%)	3rd cycle (%)	7th cycle (%)	10th cycle (%)
neat rubber	48.2	22.4	20.1	18.5	17.9
composite 1-ply	62.0	29.7	26.6	23.1	22.5
composite 4-ply	66.9	32.2	29.0	25.0	24.4

explain the mechanical behavior of the composite shown below. Four possible failures can occur. The first, mode 1, is related to the minimum angle that the braid can form due to its diameter and volume fraction (geometrical limitations) at which point the CNTYs reach their jammed state. In the second mode, mode 2, the fibers are jammed and fracture; thus, the mechanical behavior depends on the ultimate yarn strength. In mode 3, the elastomer matrix fractures, and in mode 4, there is debonding between the fibers and elastomer matrix. Only modes 1 and 4 were found in the experimental testing.

The stress–strain relationship for the elastomer tube and the braided composites is shown in Figure 6. Figure 6a shows the cyclic stress–strain behavior of a neat silicone tube and a composite tube containing single-ply CNTYs and 4-ply CNTYs for 10 cycles. As can be observed, the first cycle of loading is different from the subsequent cycles. The modulus is lower after

https://doi.org/10.1021/acsomega.2c01991
ACS Omega 2022, 7, 40766–40774

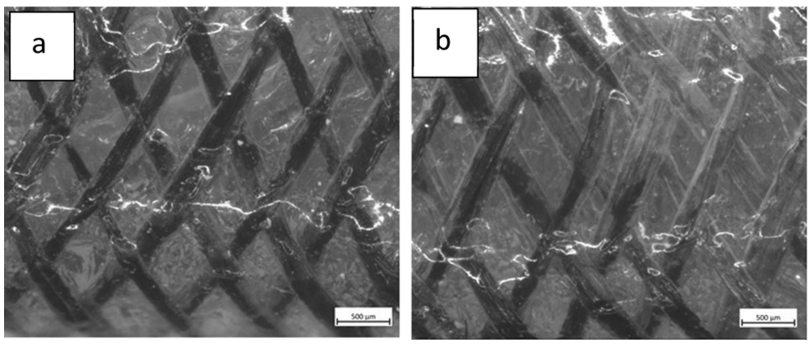

Figure 7. Picture of the braided composite (a) before and (b) after stretching.

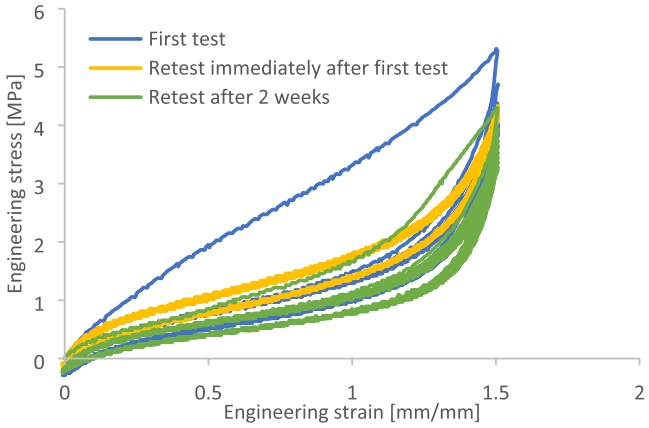

Figure 8. Stress and strain behavior of stretchable 1-ply CNTY composites with a braiding angle of 55°, first test, retesting immediately after the first 10 cycles, and testing after a recovery time of 2 weeks for additional 10 cycles.

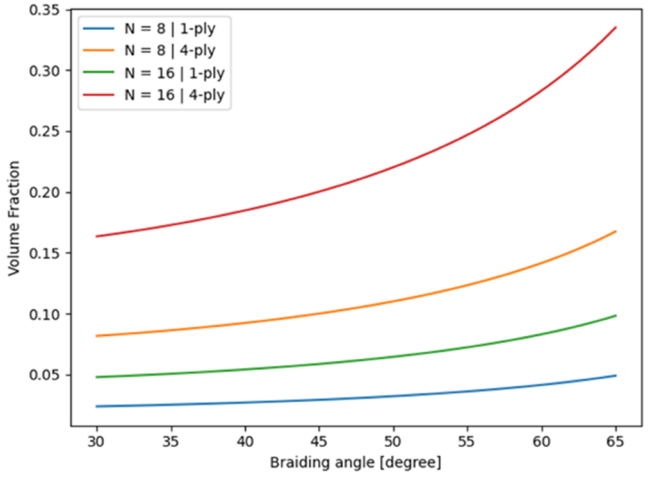

Figure 9. Relationship between the volume fraction and braiding angle for 1-ply and 4-ply with different numbers of yarns.

the first cycle (stress softening), as seen in Figure 6c (first cycle) and Figure 6d (second cycle). From Figure 5c, the stress seems similar for all of the materials after the second cycle up to a strain close to 0.7. Above this strain, there are deviations between the neat rubber and the fiber−elastomer composites, and the yarns appear to have a more significant contribution to the composite mechanical behavior. It should be noted that the 4-ply yarns have a much higher modulus compared to the 1-ply, at 46.4 and 4.9 Gpa, respectively. A strain of 0.7 appears to be the critical strain, where the yarns become jammed, and mode 1 is reached. The critical strain is dependent on the initial braiding angle of the braid (Figure 6b). Above the critical strain, debonding of the yarns from the matrix (failure mode 3) may occur.

In Figure 6a, energy loss or hysteresis is observed (difference between the loading and unloading curves). Generally, during the cycling of the silicone composites, hysteresis was observed to be the highest for the 4-ply CNTY composites and lowest for the neat silicone tube. Regardless, all materials exhibit hysteretic behavior. The hysteresis of the different tubular structures was calculated and is summarized in Table 1. Comparing the first loading cycle to the second cycle, there is a significant decrease in energy loss between the first and second cycles. For the neat elastomer, although it is expected to see very little hysteresis reduction, the presence of silica particles in the elastomer creates the expected stress softening or "Mullins effect".[36] In the case of the composite, the amount of hysteresis is significantly higher than the elastomer alone for the first cycle. The large decrease in the hysteresis value for the composite may indicate debonding between the yarns and the matrix on the first cycle. While the first cycle is significantly higher than the second cycle, there is still some decrease due to the elastomer from the second cycle onward. While the actual area between the loading and unloading curves is affected by the modulus, as demonstrated by the 4-ply composite, the relative decrease between the 4-ply composite (24%) and the 1-ply composite (24%) is nearly the same as the elastomer (20%) between cycles 2 and 10. While there may be some additional debonding, the hysteresis behavior is governed predominantly by the elastomer over cycles 2−10.

To assess if debonding was occurring, samples were investigated by optical microscopy. Figure 7 shows the composite before and after stretching. As observed in Figure 7, after stretching, a separation between the matrix and the yarns occurs.

To further evaluate if the first cycle hysteresis was caused by fiber−matrix debonding, the loaded samples were left to recover for 2 weeks and then loaded again. If fiber−matrix debonding was the cause, it would not be recovered. As can be seen in Figure 8, the sample after 2 weeks of recovery showed the typical stress softening of elastomers, but the very large first cycle hysteretic behavior was no longer present. This supports the hypothesis that the first cycle hysteresis was caused by the fiber−matrix debonding. However, it should be noticed by the experimental results that debonding (after the first cycle) did not cause further change in the stress−strain behavior upon mechanical cycling. This may be attributed to mechanical interlocking and friction between the brain and the elastomeric matrix. A debonding between the fiber and the matrix could be

https://doi.org/10.1021/acsomega.2c01991
ACS Omega 2022, 7, 40766−40774

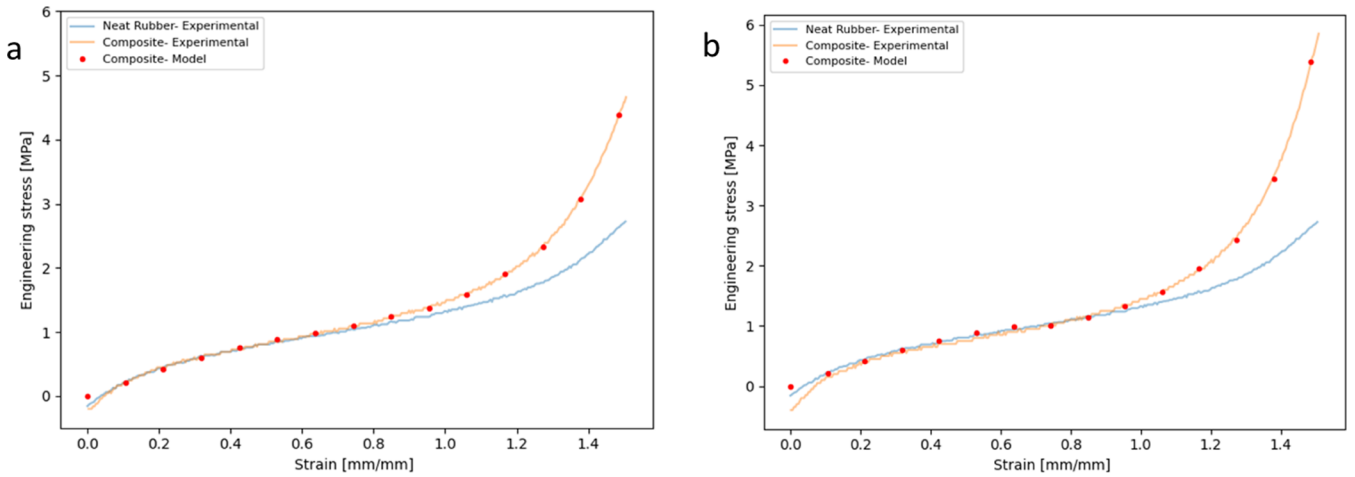

Figure 10. Experimental engineering stress vs strain for the neat tubular elastomer, the CNTY composites, and the calculated results (dots) with a braiding angle of 55°: (a) 1-ply composite and (b) 4-ply composite.

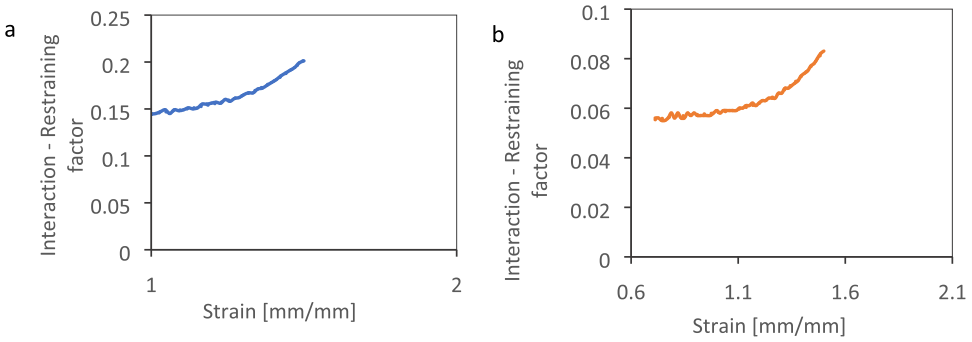

Figure 11. Relationship of the interaction-restraining factors with strain for (a) 1-ply and (b) 4-ply composites.

Table 2. Average Value of the Resistivities and Conductivities for 4-ply and 1-ply Composites

	resistivity (Ω·cm)	conductivity (S cm^{-1})	SD
1-ply	5.01×10^{-4}	1.99×10^{3}	1.87×10^{-6}
4-ply	5.67×10^{-5}	1.76×10^{4}	1.45×10^{-6}

avoided by improving the adhesion between the two by physical bonds such as a coupling agent or by covalent bonds by treating the fiber in advance with a functional group that could cure and react with the matrix.

The volume fractions of the braided composites were calculated according to eq 3 and are shown in Figure 9 for 8 and 16 yarns with 4-ply yarns and 1-ply yarns vs the braiding angles. As the number of yarns increases or the diameter of the yarns increases (4-ply vs 1-ply), the fiber fractional volume increases. For a braiding angle of 55°, the volume fraction of 1-ply with 8 and 16 yarns is 0.024 and 0.082, respectively, and for 4-ply with 8 and 16 yarns, it is 0.047 and 0.163, respectively.

Figure 10 presents the theoretical and experimental stress−strain curves for the tubular neat and braid composites. As

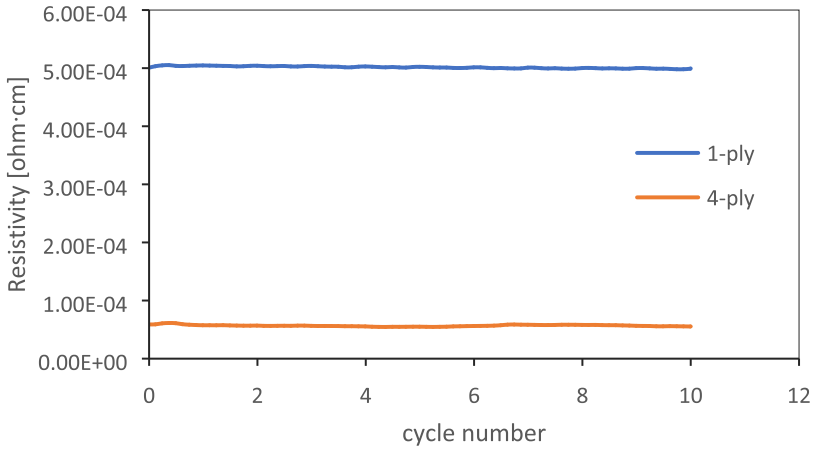

Figure 12. Resistivities vs cycle number during the tensile test for 4-ply and 1-ply composites.

https://doi.org/10.1021/acsomega.2c01991
ACS Omega 2022, 7, 40766−40774

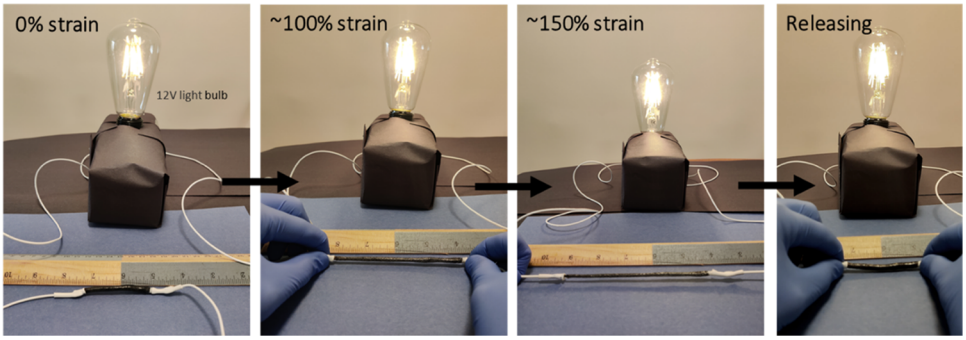

Figure 13. LED lamps integrated with stretchable CNTY composite interconnection during stretching deformation.

shown, there is good agreement between the theoretical calculations and the experimental results for both 1-ply (Figure 10a) and 4-ply (Figure 10b) yarns, provided the interaction parameter is included in the second loading region. The interaction parameter as a function of strain for the different composites is shown in Figure 11. The trend of the interaction parameter as a function of strain (increases with strain) seems to be similar for both systems, but the actual value of the interaction factor will change for different yarns, as seen in Figure 11.

The resistivities and conductivities of the composite were calculated based on the yarns' measured resistance, length, and cross-sectional area. The average values over 10 cycles are shown in Table 2. For comparison, the resistivity and conductivity of copper are 1.6×10^{-6} Ω·cm and 5.9×10^{5} S cm^{-1}, respectively. The calculations do not consider the change in the cross section of the yarns during extension. The values are in good agreement with the electrical properties of the yarns provided by the manufacturer, and the fabrication of the composite and stretching do not damage the electrical properties (Figure 12).

Finally, to demonstrate the continuity and stability of the electrical conductivity of the braided elastomeric tubes, a demonstration circuit was prepared composed of the stretchable tube, a 12 V battery, and a light-emitting diode (LED) bulb. As evident from Figure 13, the level of the LED brightness was kept stable and constant when stretching to 150% and upon release of the load and repeated loadings.

CONCLUSIONS

In this work, a novel composite characterized by high stretch to 150% and possessing constant stable conductivity was investigated. The approach used a braided CNTY tubular structure embedded in an elastomer matrix.

The resistivity and conductivity of the composite were 5.01×10^{-4} Ω·cm and 1.99×10^{3} S cm^{-1}, respectively; for the 1-ply CNTY-containing composite and for the 4-ply CNTY-based composite, the resistivity and conductivity were 5.67×10^{-5} Ω·cm and 1.76×10^{4} S cm^{-1}, respectively. The values were maintained up to 150% axial stretch and over 10 cycles. These values are considered in the range from the conductive material to the semiconductive material. Thus, this tubular geometry shows promise for stretchable electronics applications requiring stable and constant electrical properties with stretch.

A composite hyperelastic model for large deformations was developed based on the strain energy density function and braid geometry to describe the deformation−stress relationship of this elastomer-reinforced braided CNTY composite tube. An interaction parameter was proposed to account for the rubber matrix and reinforcing yarn interaction and friction. The proposed model shows good agreement with the experimental results.

Since the tubular geometry limits the stretchability, different geometries should be considered for future work with the aim to increase the stretching limit beyond 200%.

ASSOCIATED CONTENT

Supporting Information

The Supporting Information is available free of charge at https://pubs.acs.org/doi/10.1021/acsomega.2c01991.

Additional experimental details, equation development, and photographs, as follows: development of the volume fraction of the yarns equation; calculation of the braided area; optical microscopy images of failure modes of the composite braid structure; and electrical conductivity of pure CNT yarns under stretching (PDF)

AUTHOR INFORMATION

Corresponding Author

Avia J. Bar − *Department of Plastics Engineering, University of Massachusetts Lowell, Lowell, Massachusetts 01854, United States;* orcid.org/0000-0003-4088-3605; Email: Avia_Bar@student.uml.edu

Authors

Joey Mead − *Department of Plastics Engineering, University of Massachusetts Lowell, Lowell, Massachusetts 01854, United States;* orcid.org/0000-0003-0631-859X

Hanna Dodiuk − *Department of Polymers and Plastics Engineering, Shenkar College of Engineering and Design, Ramat-Gen 52526, Israel*

Samuel Kenig − *Department of Polymers and Plastics Engineering, Shenkar College of Engineering and Design, Ramat-Gen 52526, Israel*

Complete contact information is available at: https://pubs.acs.org/10.1021/acsomega.2c01991

Author Contributions

S.K., J.M., H.D., and A.J.B. contributed to the design of the work and interpretation of the data. A.J.B. was involved in the acquisition, analysis, the creation of new software used in the work, and manuscript draft.

Funding

The David and Frances Pernick foundation sponsored the graduate student A.J.B.

Notes

The authors declare no competing financial interest.

■ ACKNOWLEDGMENTS

The authors would like to acknowledge Nanocomp for supplying the CNTYs and Wardwell braiding for the braiding machine.

■ ABBREVIATIONS

CNTYs, carbon nanotube yarns; PDMS, poly-(dimethylsiloxane); CLPT, classical laminate plate theory; FGM, fabric geometry models; FEA, finite-element analysis; VA, volume averaging methods

■ REFERENCES

(1) Lacour, S. P.; Wagner, S.; Huang, Z.; Suo, Z. Stretchable Gold Conductors on Elastomeric Substrates. *Appl. Phys. Lett.* **2003**, *82*, 2404−2406.
(2) Cai, L.; Wang, C. Carbon Nanotube Flexible and Stretchable Electronics. *Nanoscale Res. Lett.* **2015**, *10*, No. 320.
(3) Ma, Y.; Feng, X.; Rogers, J. A.; Huang, Y.; Zhang, Y. Design and Application of "J-Shaped" Stress−Strain Behavior in Stretchable Electronics: A Review. *Lab Chip* **2017**, *17*, 1689−1704.
(4) Ahn, J. H.; Je, J. H. Stretchable Electronics: Materials, Architectures and Integrations. *J. Phys. D: Appl. Phys.* **2012**, *45*, No. 103001.
(5) Kim, D. C.; Shim, H. J.; Lee, W.; Koo, J. H.; Kim, D.-H. Stretchable Electronics: Material-Based Approaches for the Fabrication of Stretchable Electronics (Adv. Mater. 15/2020). *Adv. Mater.* **2020**, *32*, No. 2070118.
(6) Hammock, M. L.; Chortos, A.; Tee, B. C.-K.; Tok, J. B.-H.; Bao, Z. 25th Anniversary Article: The Evolution of Electronic Skin (E-Skin): A Brief History, Design Considerations, and Recent Progress. *Adv. Mater.* **2013**, *25*, 5997−6038.
(7) Webb, R. C.; Bonifas, A. P.; Behnaz, A.; Zhang, Y.; Yu, K. J.; Cheng, H.; Shi, M.; Bian, Z.; Liu, Z.; Kim, Y.-S.; Yeo, W.-H.; Park, J. S.; Song, J.; Li, Y.; Huang, Y.; Gorbach, A. M.; Rogers, J. A. Ultrathin Conformal Devices for Precise and Continuous Thermal Characterization of Human Skin. *Nat. Mater.* **2013**, *12*, 938−944.
(8) Wang, Y.; Wang, L.; Yang, T.; Li, X.; Zang, X.; Zhu, M.; Wang, K.; Wu, D.; Zhu, H. Wearable and Highly Sensitive Graphene Strain Sensors for Human Motion Monitoring. *Adv. Funct. Mater.* **2014**, *24*, 4666−4670.
(9) Son, D.; Lee, J.; Qiao, S.; Ghaffari, R.; Kim, J.; Lee, J. E.; Song, C.; Kim, S. J.; Lee, D. J.; Jun, S. W.; Yang, S.; Park, M.; Shin, J.; Do, K.; Lee, M.; Kang, K.; Hwang, C. S.; Lu, N.; Hyeon, T.; Kim, D.-H. Multifunctional Wearable Devices for Diagnosis and Therapy of Movement Disorders. *Nat. Nanotechnol.* **2014**, *9*, 397−404.
(10) Choong, C.-L.; Shim, M.-B.; Lee, B.-S.; Jeon, S.; Ko, D.-S.; Kang, T.-H.; Bae, J.; Lee, S. H.; Byun, K.-E.; Im, J.; Jeong, Y. J.; Park, C. E.; Park, J.-J.; Chung, U.-I. Highly Stretchable Resistive Pressure Sensors Using a Conductive Elastomeric Composite on a Micropyramid Array. *Adv. Mater.* **2014**, *26*, 3451−3458.
(11) Yeo, W.-H.; Kim, Y.-S.; Lee, J.; Ameen, A.; Shi, L.; Li, M.; Wang, S.; Ma, R.; Jin, S. H.; Kang, Z.; Huang, Y.; Rogers, J. A. Multifunctional Epidermal Electronics Printed Directly onto the Skin. *Adv. Mater.* **2013**, *25*, 2773−2778.
(12) Lee, S. K.; Kim, B. J.; Jang, H.; Yoon, S. C.; Lee, C.; Hong, B. H.; Rogers, J. A.; Cho, J. H.; Ahn, J. H. Stretchable Graphene Transistors with Printed Dielectrics and Gate Electrodes. *Nano Lett.* **2011**, *11*, 4642−4646.
(13) Tee, B. C.-K.; Chortos, A.; Berndt, A.; Nguyen, A. K.; Tom, A.; McGuire, A.; Lin, Z. C.; Tien, K.; Bae, W.-G.; Wang, H.; Mei, P.; Chou, H.-H.; Cui, B.; Deisseroth, K.; Ng, T. N.; Bao, Z. A Skin-Inspired Organic Digital Mechanoreceptor. *Science* **2015**, *350*, 313−316.
(14) Lim, S.; Son, D.; Kim, J.; Lee, Y. B.; Song, J.-K.; Choi, S.; Lee, D. J.; Kim, J. H.; Lee, M.; Hyeon, T.; Kim, D.-H. Transparent and Stretchable Interactive Human Machine Interface Based on Patterned Graphene Heterostructures. *Adv. Funct. Mater.* **2015**, *25*, 375−383.
(15) Stoppa, M.; Chiolerio, A. Wearable Electronics and Smart Textiles: A Critical Review. *Sensors* **2014**, *14*, 11957−11992.
(16) Sim, K.; Rao, Z.; Ershad, F.; Yu, C. Rubbery Electronics Fully Made of Stretchable Elastomeric Electronic Materials. *Adv. Mater.* **2020**, *32*, No. 1902417.
(17) Kim, D. C.; Shim, H. J.; Lee, W.; Koo, J. H.; Kim, D. H. Material-Based Approaches for the Fabrication of Stretchable Electronics. *Adv. Mater.* **2020**, *32*, No. 1902743.
(18) Ko, S. H.; Lee, Z. W. D.*Flexible and Stretchable Electronics*; MDPI, 2018.
(19) Taya, M.; Kim, W. J.; Ono, K. Piezoresistivity of a Short Fiber/Elastomer Matrix Composite. *Mech. Mater.* **1998**, *28*, 53−59.
(20) Harkleroad, W. I. Basic Principles of Hose Design. *Rubber Chem. Technol.* **1969**, *42*, 666−674.
(21) Shang, Z.; Wang, S.; You, Z.; Ma, J. A Hybrid Tubular Braid With Improved Longitudinal Stiffness For Medical Catheter. *J. Mech. Med. Biol.* **2019**, *19*, No. 1950003.
(22) Fujihara, K.; Teo, K.; Gopal, R.; Loh, P. L.; Ganesh, V. K.; Ramakrishna, S.; Foong, K. W. C.; Chew, C. L. Fibrous Composite Materials in Dentistry and Orthopaedics: Review and Applications. *Compos. Sci. Technol.* **2004**, *64*, 775−788.
(23) Mouritz, A. P.; Bannister, M. K.; Falzon, P. J.; Leong, K. H. Review of Applications for Advanced Three-Dimensional Fibre Textile Composites. *Composites, Part A* **1999**, *30*, 1445−1461.
(24) Lötters, J. C.; Olthuis, W.; Veltink, P. H.; Bergveld, P. The Mechanical Properties of the Rubber Elastic Polymer Polydimethylsiloxane for Sensor Applications. *J. Micromech. Microeng.* **1997**, *7*, 145−147.
(25) Nour, M.; Berean, K.; Griffin, M. J.; Matthews, G. I.; Bhaskaran, M.; Sriram, S.; Kalantar-Zadeh, K. Nanocomposite Carbon-PDMS Membranes for Gas Separation. *Sens. Actuators, B* **2012**, *161*, 982−988.
(26) MIRALON: Huntsman Corporation (HUN). https://www.huntsman.com/products/detail/344/miralon/yarn (accessed May 10, 2021).
(27) Carey, J. P.; Melenka, G. W.; Hunt, A. J.; Ayranci, C.Introduction to Braided Composite Material Behavior. In *Handbook of Advances in Braided Composite Materials*; Elsevier, 2017; Chapter 5, pp 207−237.
(28) Peng, X.; Guo, G.; Zhao, N. An Anisotropic Hyperelastic Constitutive Model with Shear Interaction for Cord-Rubber Composites. *Compos. Sci. Technol.* **2013**, *78*, 69−74.
(29) Cho, J. R.; Yoon, Y. H.; Seo, C. W.; Kim, Y. G. Fatigue Life Assessment of Fabric Braided Composite Rubber Hose in Complicated Large Deformation Cyclic Motion. *Finite Elem. Anal. Des.* **2015**, *100*, 65−76.
(30) Yang, H.; Yao, X. F.; Ke, Y. C.; Ma, Y.-j.; Liu, Y. H. Constitutive Behaviors and Mechanical Characterizations of Fabric Reinforced Rubber Composites. *Compos. Struct.* **2016**, *152*, 117−123.
(31) Xu, X.; Yao, X.; Dong, Y.; Yang, H.; Yan, H. Mechanical Behaviors of Non-Orthogonal Fabric Rubber Seal. *Compos. Struct.* **2021**, *259*, No. 113453.
(32) Yeoh, O. H. Some Forms of the Strain Energy Function for Rubber. *Rubber Chem. Technol.* **1993**, *66*, 754−771.
(33) Rawal, A.; Saraswat, H.; Kumar, R. Tensile Response of Tubular Braids with an Elastic Core. *Composites, Part A* **2013**, *47*, 150−155.
(34) Rawal, A.; Sibal, A.; Saraswat, H.; Khan, S. Q. Topologically Controlled Tensile Behaviour of Braided Prostheses for Anterior Cruciate Ligaments. *J. Mech. Behav. Biomed. Mater.* **2016**, *57*, 359−364.
(35) Rawal, A.; Kumar, R.; Saraswat, H. Tensile Mechanics of Braided Sutures. *Text. Res. J.* **2012**, *82*, 1703−1710.
(36) Bueche, F. Molecular Basis for the Mullins Effect. *J. Appl. Polym. Sci.* **1960**, *4*, 107−114.

https://doi.org/10.1021/acsomega.2c01991
ACS Omega 2022, 7, 40766−40774